POLITECNICO DI TORINO
Repository ISTITUZIONALE

Modeling and Experimental Characterization of a Full-Scale Electrodynamic Suspension System for High-Speed Lane-Switching

Original
Modeling and Experimental Characterization of a Full-Scale Electrodynamic Suspension System for High-Speed Lane-Switching / Kleikemper, O., Pakstys, M., Rink, S., Radeck, D., Tonoli, A., Holzapfel, F.. - In: IEEE TRANSACTIONS ON MAGNETICS. - ISSN 0018-9464. - (2026). [10.1109/tmag.2026.3689606]

Availability:
This version is available at: 11583/3015748 since: 2026-09-21T09:42:18Z

Publisher:
Institute of Electrical and Electronics Engineers

Published
DOI:10.1109/tmag.2026.3689606

Terms of use:

This article is made available under terms and conditions as specified in the corresponding bibliographic description in the repository

Publisher copyright

(Article begins on next page)

01 November 2026

This article has been accepted for publication in IEEE Transactions on Magnetics. This is the author's version which has not been fully edited and content may change prior to final publication. Citation information: DOI 10.1109/TMAG.2026.3689606

Modeling and Experimental Characterization of a Full-Scale Electrodynamic Suspension System for High-Speed Lane-Switching

Oliver Kleikemper[1], Marius Pakštys[2], Sebastian Rink[1], Domenik Radeck[1], Andrea Tonoli[2], Florian Holzapfel[3]
[1]TUM Hyperloop, Technical University of Munich, 85521 Ottobrunn, Germany, oliver.kleikemper@tum.de
[2]Department of Mechanical and Aerospace Engineering, Politecnico di Torino, 10129 Turin, Italy
[3]Institute of Flight System Dynamics, Technical University of Munich, 85748 Garching, Germany

Lane-switching in maglev systems is a key functionality necessary for their successful implementation in commercial solutions, that has largely remained unexplored in terms of experimental validation. The present work investigates a full-scale electrodynamic suspension for its use alongside a conventional electromagnetic suspension. A combined levitation system that incorporates the repulsive force of an electrodynamic suspension and the attraction-based behavior of an electromagnetic suspension facilitates high-speed vertical lane-switching capability. The passivity of electrodynamic suspensions renders them appealing for their integration in this context. A test bench designed for full-scale analysis of this process is presented. The electrodynamic suspension system is discussed, and a finite element model used for system design is established. Acquired experimental lift and drag forces are fitted using an analytical model consisting of an equivalent multi-branch electric circuit, showing good agreement between datasets. A large speed range (10-600 km/h) is tested over several air gaps (35-50 mm). Measurements at smaller air gaps (25 and 30 mm) are used to validate the analytical model. Moreover, full-scale force capability necessary for vehicle levitation is achieved.

***Index Terms*—Electrodynamic levitation, full-scale test bench, lane-switching, maglev, modeling**

I. Introduction

ELECTRODYNAMIC suspension (EDS) has seen increased interest over the past decade due to its passive operation and light-weight implementation, representing an enabler for magnetically levitated vehicles. Permanent magnets (PM) arranged in a Halbach array produce a unilaterally concentrated magnetic field which, when moving at non-zero speed relative to a non-ferrous conductive track, induces eddy currents in the track and generates the associated Lorentz forces [1]. Lift (repulsive) and drag forces are experienced by the moving array. Lane-switching is a challenge for conventional EMS systems where certain solutions show drawbacks. However, a separate EDS system can facilitate switching. The proposed switch configuration is defined by a vertical selection of possible directions that requires a combined levitation system that enables both attraction-based and repulsive forces [2]. In this context, a maglev vehicle bogie is outfitted with PM Halbach arrays on its underside and electromagnets on its topside. The EMS system interacts with a corresponding top-side iron rail while the EDS is designed to support the vehicle from below when interacting with the bottom aluminum rail. During the vertical lane-switch procedure, the EMS system is disengaged, lowering the vehicle onto the aluminum track to access the bottom lane. The EDS system temporarily supports the vehicle before a new EMS rail is introduced and the EMS system is engaged once again, shown schematically in Fig. 1. Due to predominantly vertical forces and negligible lateral forces in the switch, the proposed concept focuses on the levitation system. This solution decouples lateral guidance and switching functions and saves a considerable amount of vehicle mass compared with alternative arrangements such as double-EMS concepts [2]. The procedure is aimed to work for speeds between 100 and 600 km/h.

Oliver Kleikemper and Marius Pakštys contributed equally to this work.

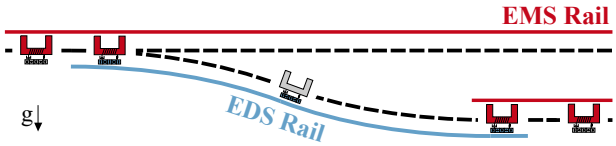


Fig. 1. Layout of vertical lane switch combining EMS and EDS capabilities. Acceleration due to gravity denoted with g.

The controlled operational transition between EMS and EDS levitation requires detailed investigation. Previous work has examined both systems independently in maglev applications. Comprehensive analyses of the EMS system are presented in [3] and [4], while analytical modeling and experimental validation of a small-scale EDS system is reported in [5], concerning static characterization. Other studies have investigated the EDS phenomenon, employing hybrid analytical modeling and partial equivalent circuits [6], [7]. These approaches are limited by their dependency on boundary conditions regarding solution quality and an increased computation time for finer mesh grids. Moreover, experimental validation in [7] is made on a small-scale test bench.

A full-scale experimental investigation of an EDS system suitable for integration into a combined EMS–EDS configuration has not yet been reported. In particular, experimental lift and drag measurements at high speeds remain limited. Prior studies have presented static measurements for various PM array–flywheel configurations [8]–[10]. While [8], [9] report measurements up to 260 km/h, [10] investigates multiple scaled configurations. Stabilization aspects of levitating EDS systems are addressed in [11]. Small-scale lift and drag force testing is also carried out in [12], reaching a maximum speed of approximately 25 km/h. Nevertheless, full-scale measurements at speeds up to 600 km/h are lacking in literature.

To address these gaps, the EMS test bench introduced in [3] is extended by integrating rotating aluminum flywheels

This work is licensed under a Creative Commons Attribution 4.0 License. For more information, see https://creativecommons.org/licenses/by/4.0/

This article has been accepted for publication in IEEE Transactions on Magnetics. This is the author's version which has not been fully edited and content may change prior to final publication. Citation information: DOI 10.1109/TMAG.2026.3689606

and Halbach arrays to enable EDS functionality. A key feature of the setup is the full-scale implementation of both magnetic systems: the EMS corresponds to the configuration used in the TUM Hyperloop demonstrator vehicle [3], and the EDS Halbach arrays are dimensioned to support the full vehicle load. Consequently, the obtained results are directly transferable to vehicle-level operation without upscaling. The extended test bench allows both static and dynamic investigations and is specifically designed to evaluate the lane-switching maneuver. A static characterization of the EDS system is carried out to identify the parameters of an equivalent electric circuit model, following [5], by fitting the analytical model to measurements over a wide range of constant speeds and air gaps. The same model can be used to study stability and transient phenomena. Static measurements verify full-scale EDS lift capability for lane-switching. Additionally, a finite element (FE) model implemented in COMSOL Multiphysics is presented in the scope of system design.

Our main contributions are as follows:

- Development of a full-scale hybrid EMS–EDS test bench,
- Experimental EDS lift and drag force measurements at speeds of up to $600\ \mathrm{km/h} = 166.67\ \mathrm{m/s}$,
- Formulation and validation of an equivalent circuit-based model,
- Demonstration of strong agreement between experimental and analytical results.

The remainder of the manuscript is organized as follows. Section II presents FE modeling and the analytical approaches. Section III describes the experimental setup and test bench. Analytical model correspondence with experimental results is discussed in Section IV. Finally, Section V concludes the paper.

II. Modeling

The EDS system is modeled in finite elements at the design stage, estimating forces and providing insight on rail eddy current density. Additionally, the system is represented by an analytical model to reproduce lift and drag forces at a wide range of constant speeds and air gaps. Its parametrization is driven by EDS system features and experimentally acquired forces. Due to its computational efficiency, the analytical model is subsequently used to characterize the EDS system.

A. Finite elements

The FE model is assembled in three dimensions using COMSOL Multiphysics, employing the AC/DC module. Figure 2 indicates the designed experimental EDS system. Geometry and features reflect that of the designed array and rail, with details reported in Table I. The curved Halbach array ensures an almost constant air gap along its arc length for different air gaps. Crucially, the geometry adequately reproduces forces experienced in a planar array. The mesh features an average skewness of 0.66. The model is computed in stationary conditions, solving for the magnetic vector potential $\mathbf{A}$ and the electric potential V in the following expression set:

$$\nabla \cdot \mathbf{J} = 0 \tag{1}$$

$$\nabla \times \mathbf{H} = \mathbf{J} \tag{2}$$

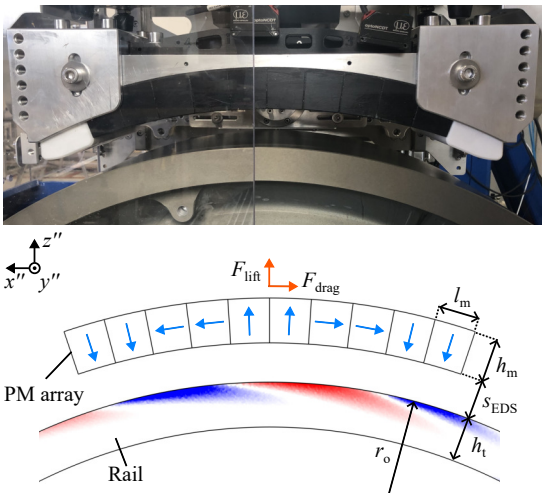


Fig. 2. Top: experimental EDS subsystem designed for lane-switch testing positioned at $s_{\mathrm{EDS}} = 35$ mm. Bottom: array cross-section with magnetization scheme and out-of-plane track eddy current component visualization at $v = 100$ km/h and $s_{\mathrm{EDS}} = 35$ mm as computed by the FE model. Track rotates clockwise producing lift F_{lift} and drag F_{drag} on the array.

$$\mathbf{B} = \nabla \times \mathbf{A} \tag{3}$$

$$\mathbf{E} = -\nabla V \tag{4}$$

$$\mathbf{J} = \sigma_{\mathrm{t}}\mathbf{E} + \sigma_{\mathrm{t}}\mathbf{v} \times \mathbf{B}. \tag{5}$$

The eddy current density is $\mathbf{J}$, and $\mathbf{H}$ is the magnetic field strength. The magnetic flux density is $\mathbf{B}$ and the electric field is denoted with $\mathbf{E}$. The velocity field $\mathbf{v}$ is required to generate an eddy current density in the rail with conductivity σ_{t}. The magnetization orientation and the computed out-of-plane eddy current density component for a speed of $v = 100$ km/h and air gap $s_{\mathrm{EDS}} = 35$ mm are also reported in Fig. 2. The model requires approximately 57 minutes to compute this operating condition, using the following resources: Intel Core i7 processor (4 cores) and 32 GB of RAM. Note that skin depth is smaller than rail thickness. Therefore, rail thickness was limited to 15 mm at the design stage to reduce computational costs.

TABLE I
EDS System Features

Parameter	Symbol	Value	Unit
Magnet width	w_{m}	150	mm
Magnet height	h_{m}	40	mm
Magnet length	l_{m}	36	mm
Magnet remanent flux density	B_{r}	1.38	T
Magnet relative permeability	μ_{r}	1.05	–
Outer track radius	r_{o}	500	mm
Rail thickness	h_{t}	35	mm
Rail width	w_{t}	168	mm
Assumed track conductivity	σ_{t}	25	MS/m

In this context, the FE model was exploited as a preliminary tool in selecting key test bench components. Note that further model tuning lies outside the scope of the present work, as FE output is influenced by variations in material properties and thermal phenomena. Moreover, computational efficiency of the analytical model strongly motivates its use in subsequent analyses, as adopted in the approach of [5].

This work is licensed under a Creative Commons Attribution 4.0 License. For more information, see https://creativecommons.org/licenses/by/4.0/

This article has been accepted for publication in IEEE Transactions on Magnetics. This is the author's version which has not been fully edited and content may change prior to final publication. Citation information: DOI 10.1109/TMAG.2026.3689606

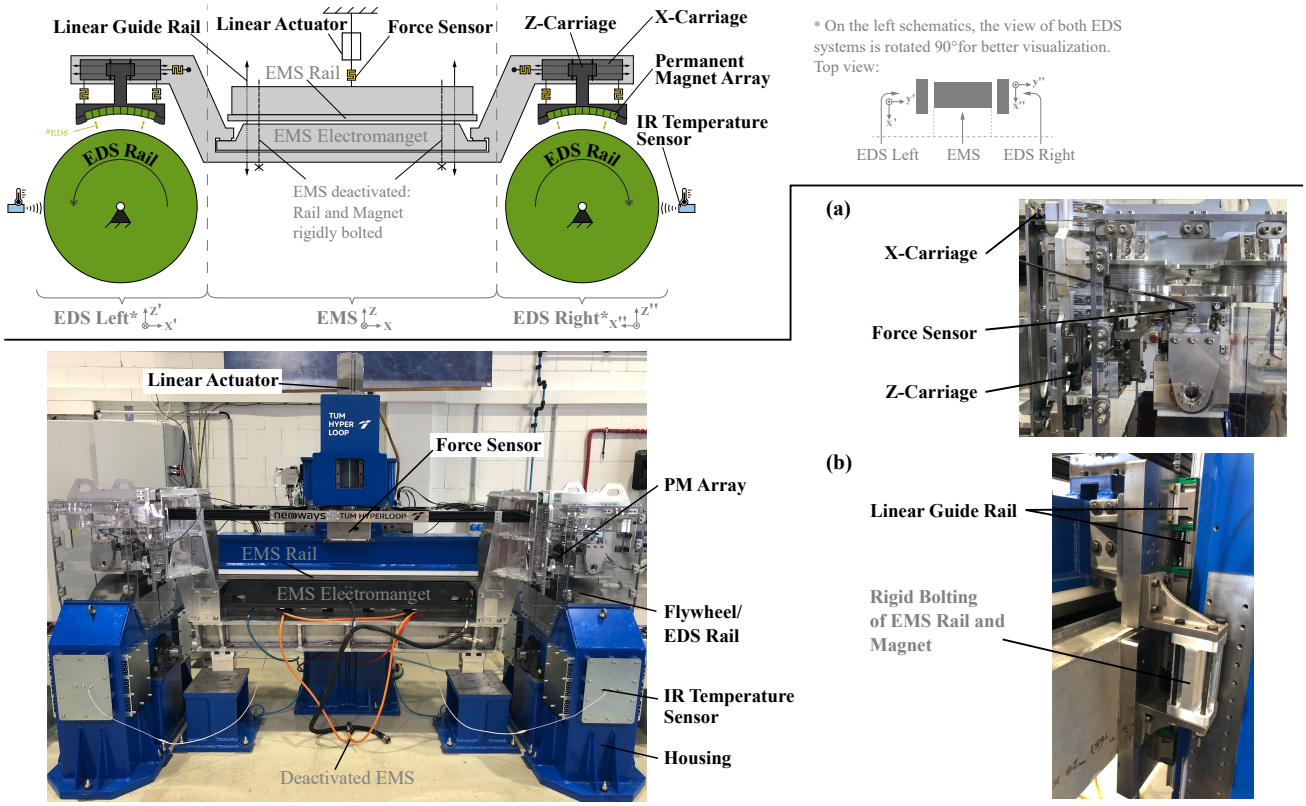


Fig. 3. Top: schematic of test bench for hybrid EMS-EDS lane-switch testing in its EDS characterization configuration. Bottom left: frontal photograph of the test bench. Bottom right (a): zoomed frontal view of PM array-rail subsystem with carriages and force sensor. Bottom right (b): central part from behind at an angle. The deactivated EMS system components are labeled in grey.

B. Analytical

The analytical model used for data fitting relies on an equivalent multi-branch electric circuit to reproduce the EDS phenomenon [1], [5]. The circuit consists of a voltage source representing the back-electromotive force E_b, with N_b parallel branches of resistances R_k and inductances L_k, themselves arranged in series. Each branch is characterized by an electrodynamic pole frequency: $\omega_{\mathrm{p},k} = R_k/L_k$. The model is an abstract representation where branches describe equivalent eddy current behavior with varying frequency content at different speeds, also capturing the skin effect. Applying Kirchhoff's voltage law on the k-th branch yields the general expression for a fixed reference frame considering branch currents i_k:

$$L_k \frac{\mathrm{d}i_k}{\mathrm{d}t} + R_k i_k + E_\mathrm{b} = 0 \tag{6}$$

with the back-electromotive force defined as

$$E_\mathrm{b} = \frac{\partial \Lambda}{\partial s_\mathrm{EDS}} \dot{s}_\mathrm{EDS} \mathrm{e}^{\mathrm{j}\omega t} + \mathrm{j}\omega \Lambda \mathrm{e}^{\mathrm{j}\omega t}. \tag{7}$$

The back-electromotive force is dependent on the periodic flux linkage Λ, itself a function of air gap s_EDS. The imaginary unit is j, time is denoted with t and excitation frequency is ω. The flux linkage is given by

$$\Lambda = \Lambda_0 \, \mathrm{e}^{-s_\mathrm{EDS}/\gamma} \tag{8}$$

with Λ_0 being the flux linkage amplitude. The magnetic pole pitch ratio is defined with

$$\gamma = \frac{N_\mathrm{p} l_\mathrm{m}}{\pi} \tag{9}$$

depending on the number of poles N_p and the length of one pole $2l_\mathrm{m}$ (consisting of two adjacent and identical PMs of length l_m as seen in the FE model schematic of Fig. 2). Pole length is parallel to longitudinal motion. Note that excitation frequency $\omega = v/\gamma$ is a function of longitudinal speed v and the magnetic pole pitch ratio. In a rotating reference frame, the transformation $i_k = i_{\mathrm{r},k}\mathrm{e}^{\mathrm{j}\omega t}$ allows for a simplification of (6) when substituting (7) for the back-electromotive force, resulting in

$$L_k \frac{\mathrm{d}i_{\mathrm{r},k}}{\mathrm{d}t} + R_k i_{\mathrm{r},k} + \mathrm{j}\omega L_k i_{\mathrm{r},k} + \frac{\partial \Lambda}{\partial s_\mathrm{EDS}} \dot{s}_\mathrm{EDS} + \mathrm{j}\omega \Lambda = 0. \tag{10}$$

The following relation expresses direct and quadrature components ($i_{\mathrm{d},k}$ and $i_{\mathrm{q},k}$, respectively) of the rotating current vector: $i_{\mathrm{r},k} = i_{\mathrm{d},k} + \mathrm{j}i_{\mathrm{q},k}$. Its substitution into (10) leads to the subsequent coupled equations:

$$\frac{\mathrm{d}i_{\mathrm{d},k}}{\mathrm{d}t} = -\omega_{\mathrm{p},k} i_{\mathrm{d},k} + \omega i_{\mathrm{q},k} - \frac{\partial \Lambda}{\partial s_\mathrm{EDS}} \frac{\dot{s}_\mathrm{EDS}}{L_k} \tag{11}$$

$$\frac{\mathrm{d}i_{\mathrm{q},k}}{\mathrm{d}t} = -\omega_{\mathrm{p},k} i_{\mathrm{q},k} - \omega i_{\mathrm{d},k} - \frac{\Lambda \omega}{L_k}. \tag{12}$$

To identify mechanical contributions, (11) and (12) are multiplied by $i_{\mathrm{d},k}$ and $i_{\mathrm{q},k}$, respectively. The two resulting expres-

This work is licensed under a Creative Commons Attribution 4.0 License. For more information, see https://creativecommons.org/licenses/by/4.0/

This article has been accepted for publication in IEEE Transactions on Magnetics. This is the author's version which has not been fully edited and content may change prior to final publication. Citation information: DOI 10.1109/TMAG.2026.3689606

sions are summed, representing the power balance of branch k. Consequently, general lift and drag forces are

$$F_{\mathrm{lift}} = \frac{\partial \Lambda}{\partial s_{\mathrm{EDS}}} \sum_{k=1}^{N_{\mathrm{b}}} i_{\mathrm{d},k} \tag{13}$$

$$F_{\mathrm{drag}} = -\frac{\Lambda}{\gamma} \sum_{k=1}^{N_{\mathrm{b}}} i_{\mathrm{q},k} \tag{14}$$

and considering expressions (11) and (12) in static conditions gives lift and drag forces at constant speed:

$$F_{\mathrm{lift,s}} = \frac{\Lambda_0^2}{\gamma} \, \mathrm{e}^{-2 s_{\mathrm{EDS}}/\gamma} \sum_{k=1}^{N_{\mathrm{b}}} \frac{\omega^2/\omega_{\mathrm{p},k}^2}{L_k(1+\omega^2/\omega_{\mathrm{p},k}^2)} \tag{15}$$

$$F_{\mathrm{drag,s}} = \frac{\Lambda_0^2}{\gamma} \, \mathrm{e}^{-2 s_{\mathrm{EDS}}/\gamma} \sum_{k=1}^{N_{\mathrm{b}}} \frac{\omega/\omega_{\mathrm{p},k}}{L_k(1+\omega^2/\omega_{\mathrm{p},k}^2)}. \tag{16}$$

III. Test bench and experimental setup

The test bench presented in [3] is now extended with EDS functionality, shown in the schematic (top) and image (bottom left) of Fig. 3. In particular, on both sides of the central EMS system, an EDS system in the form of a flywheel and PM array configuration is added (EDS Left and EDS Right in the schematic). The symmetric arrangement avoids unfavorable loads on the EMS structure and linear guides. The relative velocity v between vehicle and track is introduced as peripheral speeds of the two aluminum flywheels (AW2618A-T652 alloy) simulating the EDS rail. They have a radius of 0.5 m, a rail thickness of $h_{\mathrm{t}} = 35$ mm and width of $w_{\mathrm{t}} = 168$ mm. Their axes are parallel to the image plane and foundation in Fig. 3 (bottom left). For better visualization, the associated schematic (top) features an orthogonal axis orientation relative to the image plane. The flywheels are controlled in synchronized rotational speed using SEW DRU280MR4 motors (not depicted) and interact with onboard PM arrays (NdFeB sintered N48H magnets) that are implemented with curved geometry. Table I summarizes the geometry and material parameters of flywheel and array. The flywheels are designed to withstand dynamic forces up to 700 km/h and 120 °C. Above this temperature, the material exhibits a significant reduction in 0.2 % proof stress. The flywheel and array assembly are enclosed within a protective housing to prevent external interference and to ensure safe containment during operation.

Each array is attached to a rigid frame connected to the central EMS system. The frame is designed to provide maximum stiffness under the expected loads. X- and Z-Carriages integrate force sensors (Baumer DLM40-IN and DLM40-SO) to measure the produced lift and drag forces (see bottom right (a) of Fig. 3). For the EDS characterization configuration used in the presented measurements, the EMS system is deactivated; its magnet and rail are rigidly bolted together (see bottom right (b) of Fig. 3). The complete assembly, including the PM arrays, is vertically positioned by a linear actuator, indicated in the image (bottom left) and schematic (top) of Fig. 3, which allows adjustment of the air gap s_{EDS}. An additional force sensor is installed between the assembly and the linear actuator to measure the combined lift force of both EDS systems. As the flywheel temperature rises in operation due to the generated eddy currents, infrared temperature sensors (Optris / CSmicro LT) monitor them continuously.

A state machine is implemented to automatically perform measurements at different air gaps s_{EDS} set by vertically positioning the magnet assembly and by applying different relative velocities v using the motors. Theoretically, a grid resolution of 0.01 mm for s_{EDS} and 0.05236 m/s for v can be achieved. During the procedure, lift and drag forces as well as motor parameters are recorded for each pair of (s_{EDS}, v). The optical temperature sensors are used to supervise the thermal condition of the flywheels, allowing to automatically pause the measurements when a temperature threshold is reached.

IV. Results and discussion

The modeling approach from Section II-B is implemented in an interior-point constrained minimization algorithm in MATLAB, identifying branch pole frequencies and inductances for stationary forces of one array. Forces are acquired from the experimental setup described in Section III. Identified parameters are associated to a reduced error norm between analytical and experimental datasets. Given larger lift force error magnitudes, the average lift-to-drag ratio is computed and used to scale the drag force error to avoid favoring lift force error reduction. Flux linkage amplitude Λ_0 is assumed unitary. Branch pole frequency and inductance show a variation with air gap, following the polynomial functions

$$\omega_{\mathrm{p},k} = a_k s_{\mathrm{EDS}}^3 + b_k s_{\mathrm{EDS}}^2 + c_k s_{\mathrm{EDS}} + d_k \tag{17}$$

$$L_k = e_k s_{\mathrm{EDS}}^3 + f_k s_{\mathrm{EDS}}^2 + g_k s_{\mathrm{EDS}} + h_k. \tag{18}$$

Coefficients are reported in Table II. Four electric circuit branches are necessary to reproduce force behavior over the test speed range. The number of branches accounts for electrodynamic phenomena at the wide speed and air gap ranges studied experimentally. Branch number is evaluated against force error reduction: introducing additional branches beyond a threshold yields negligible improvement.

TABLE II
Electric circuit branch parameter coefficients

Coefficient	Branch, k				Unit
	1	2	3	4	
a_k	0.45	0.83	2.14	13.1	$\mathrm{Mrad/(sm^3)}$
b_k	0.056	0.11	0.26	3.12	$\mathrm{Mrad/(sm^2)}$
c_k	−6.5	−12.5	−30.3	−277	krad/(sm)
d_k	139	346	1000	7265	rad/s
e_k	−3693	14	46	7.67	$\mathrm{H/m^3}$
f_k	365	7.86	12.3	17.7	$\mathrm{H/m^2}$
g_k	−10.9	−0.64	−1.18	−1.17	H/m
h_k	0.11	0.02	0.03	0.04	H

Figure 4 indicates experimental forces of one array with fitted analytical traces. Air gaps are bounded between 35 and 50 mm. A finer discretization of testing speeds is taken at the lower speed range to capture more prominent force variations. The traces present agreeable conformity, with an average error of 2.6 % for lift force and 1 % for drag force, across all speeds and air gaps. Note that array curvature is negligible regarding

This work is licensed under a Creative Commons Attribution 4.0 License. For more information, see https://creativecommons.org/licenses/by/4.0/

This article has been accepted for publication in IEEE Transactions on Magnetics. This is the author's version which has not been fully edited and content may change prior to final publication. Citation information: DOI 10.1109/TMAG.2026.3689606

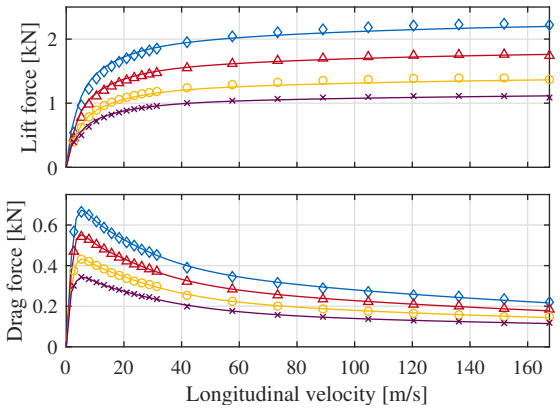


Fig. 4. Analytical lift and drag force (solid lines) of one array fitted to experimental data (markers). Air gaps of 35 (blue diamonds), 40 (red triangles), 45 (yellow circles), and 50 mm (purple crosses) are shown. Top: lift force. Bottom: drag force.

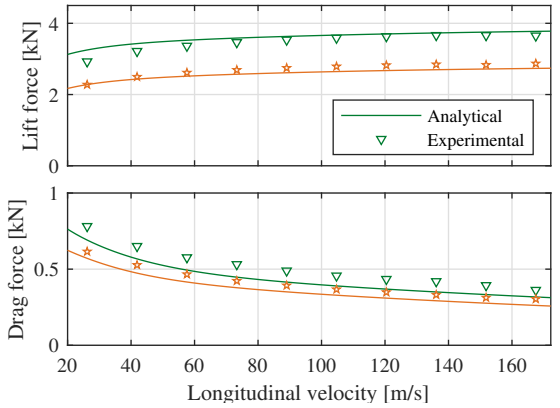


Fig. 5. Analytical lift and drag force (solid lines) of one array validated against experimental data (markers) for the following air gaps s_{EDS}: 25 (green inverted triangles) and 30 mm (orange stars). Top: lift force. Bottom: drag force.

the quality of force acquisition as well as its correspondence to a planar array.

The analytical model is further validated against experimental forces at smaller air gaps of 25 and 30 mm in Fig. 5, where it successfully replicates experimental behavior. Across the dataset, lift force shows an average error of 6 %, while drag features a greater deviation of 12 %. This error increase can be attributed to the limited samples of low air gap data in the fitting procedure, given operational speed constraints during testing. Note that data for the low speed region below 26 m/s becomes unavailable as air gap decreases, due to increasing EDS torque. A dedicated parameter set for high-speed data can be identified if required for future tests. Nevertheless, EDS system capability in producing forces necessary for full-scale levitation is shown. The estimated mass associated to the test bench mass is 640 kg, which the EMS system has been shown to levitate. Each EDS array is expected to produce lift upwards of 3.1 kN to guarantee levitation between 25-28 mm. Figure 5 indicates sufficient lift force for levitation of the test bench mass within this range, across the tested speeds. The identified EDS model is suitable for further dynamic investigation [5], where air gap oscillation is expected in the switching process.

V. Conclusion

A full-scale EDS system was designed and built to investigate a vertical lane-switching concept for a vehicle equipped with both EMS and EDS. The existing EMS test bench was extended to incorporate EDS functionality by integrating permanent magnets in a Halbach array configuration and aluminum flywheels. Using an automated measurement sequence, the lift and drag forces of the EDS system were recorded over a wide range of air gaps and relative velocities. The resulting force data were used to parametrize the proposed equivalent electric circuit model representing one array. The model predictions show excellent agreement with the experimental results. Moreover, full-scale lift force required to levitate the test bench mass is shown, corresponding to one quarter of the vehicle. The fully parametrized model can now be employed to simulate and optimize the lane-switch procedure, while its experimental dynamic investigation is planned for future work.

References

[1] R. Galluzzi, S. Circosta, N. Amati, A. Tonoli, A. Bonfitto, T. A. Lembke, and M. Kertész, "A Multi-domain Approach to the Stabilization of Electrodynamic Levitation Systems," *Journal of Vibration and Acoustics*, vol. 142, no. 6, p. 061004, 2020.

[2] D. Radeck, F. Janke, F. Gatta, J. Nicolau, G. Semino, T. Hofmann, N. König, O. Kleikemper, F. H.-M. Hsu, S. Rink, F. Achenbach, and A. Jocher, "Case study of an integrated design and technical concept for a scalable hyperloop system," *Applied System Innovation*, vol. 7, no. 6, 2024. [Online]. Available: https://www.mdpi.com/2571-5577/7/6/113

[3] O. Kleikemper, F. H.-M. Hsu, and F. Holzapfel, "Multi-mode electromagnetic suspension test bench for system characterization, model parameterization and levitation tests," *e-Prime - Advances in Electrical Engineering, Electronics and Energy*, p. 101141, 2025. [Online]. Available: https://www.sciencedirect.com/science/article/pii/S2772671125002578

[4] P. Schiefer, O. Kleikemper, and F. Holzapfel, "Modeling of Coupled Electric and Magnetic Circuits in Electromagnetic Suspension Vehicles," *IEEE Transactions on Transportation Electrification*, vol. 11, no. 1, pp. 648–655, 2025.

[5] E. Tramacere, M. Pakštys, R. Galluzzi, N. Amati, A. Tonoli, and T. A. Lembke, "Modeling and experimental validation of electrodynamic maglev systems," *Journal of Sound and Vibration*, vol. 568, p. 117950, 2024.

[6] L. Beauloye and B. Dehez, "A 3-d hybrid analytical model of a permanent magnet electrodynamic suspension," *IEEE Transactions on Energy Conversion*, vol. 40, no. 4, pp. 2843–2855, 2025.

[7] ——, "A partial element equivalent circuit model of a permanent magnet electrodynamic suspension," in *2025 IEEE Energy Conversion Conference Congress and Exposition (ECCE)*, 2025, pp. 1–8.

[8] Z. Deng, H. Shi, Z. Ke, J. Liu, Z. Li, B. Zhang, Z. Jiang, J. Zhou, and Y. Liu, "Permanent magnet electrodynamic suspension system integrated with a car: Design, implementation, and test," *IEEE Transactions on Transportation Electrification*, vol. 10, no. 1, pp. 1101–1115, 2024.

[9] H.-W. Cho, H.-S. Han, J.-S. Bang, H.-K. Sung, and B.-H. Kim, "Characteristic analysis of electrodynamic suspension device with permanent magnet halbach array," *Journal of Applied Physics*, vol. 105, no. 7, p. 07A314, 02 2009. [Online]. Available: https://doi.org/10.1063/1.3068425

[10] T. Kublin, L. Grzesiak, and M. Góźdź, "Experimental validation of a modified halbach array for improved electrodynamic suspension efficiency," *Energies*, vol. 19, no. 3, 2026. [Online]. Available: https://www.mdpi.com/1996-1073/19/3/649

[11] C. Wu, G. Li, D. Wang, and J. Xu, "Dynamic characterization of permanent magnet electrodynamic suspension system with a novel passive damping magnet scheme," *Journal of Sound and Vibration*, vol. 599, p. 118849, 2025. [Online]. Available: https://www.sciencedirect.com/science/article/pii/S0022460X24006114

[12] J. Íñiguez and V. Raposo, "Laboratory scale prototype of a low-speed electrodynamic levitation system based on a halbach magnet array," *European journal of physics*, vol. 30, no. 2, p. 367, 2009.

This work is licensed under a Creative Commons Attribution 4.0 License. For more information, see https://creativecommons.org/licenses/by/4.0/